Simulation of North Atlantic Decadal/Multidecadal Winter SST Anomalies Driven by Basin-Scale Atmospheric Circulation Anomalies

GEORGE R. HALLIWELL JR.

MPO/RSMAS, University of Miami, Miami, Florida

(Manuscript received 31 December 1995, in final form 16 September 1996)

ABSTRACT

The North Atlantic winter sea surface temperature anomaly (T_{sa}) response to anomalous surface atmospheric circulation anomalies that vary over decadal and short-term inter-decadal periods is simulated for 1950 through 1992. Anomalous ocean variability is driven by adding monthly COADS-derived anomalous fields of vector wind stress and wind speed to the climatological annual cycle forcing. A simple model is derived relating winter T_{sa} to the integrated atmospheric forcing present earlier in time that is responsible for its existence. The basin-scale structure of forced winter T_{sa} patterns depends on the structure of the atmospheric forcing along with regional differences in the dominant mixed layer processes that generate T_{sa}. For example, when the atmospheric subtropical high and subpolar low pressure systems are simultaneously strong, enhanced flow around, and baroclinic adjustments within, the subtropical gyre results in anomalously warm water in the Gulf Stream region off the U.S. East Coast. At the same time, however, the open ocean generally cools because the westerlies and trades are anomalously strong. By analyzing T_{sa} variability not driven by the atmosphere, an anomalously cold decade is identified characterized by rapid onset and termination that both occur within one year. The onset during 1968 coincides with the appearance of the great salinity anomaly, while the termination during 1977 coincides with an abrupt Northern Hemisphere climate shift that is particularly evident in the Pacific.

1. Introduction

The relative importance of different forcing mechanisms responsible for climatic sea surface temperature anomaly (T_{sa}) fluctuations in the North Atlantic depends on frequency (e.g., Bjerknes 1964; Zorita et al. 1992; Delworth et al. 1993; Deser and Blackmon 1993; Kushnir 1994). At decadal and shorter interannual periods, T_{sa} is driven primarily by the atmosphere through anomalous local air–sea fluxes. At periods of several decades, however, T_{sa} is driven primarily by changes in ocean circulation, in particular the wind-driven gyre circulation and the thermohaline meridional overturning circulation (MOC). The transition between oceanic and local atmospheric forcing thus occurs over periods between one and a few decades. Although ocean circulation oscillations are expected to influence T_{sa} significantly at these transition periods (e.g., Delworth 1993; Cai et al. 1995), a recent study (Halliwell 1997) revealed that anomalous local atmospheric forcing is important and possibly dominant during winter.

To monitor the T_{sa} response to ocean circulation changes at these transition periods, the response to atmospheric forcing must first be taken into account. To do this, Halliwell (1997) followed the life history of individual North Atlantic surface atmospheric circulation anomaly features that were responsible for driving decadal and short-term interdecadal variability in winter T_{sa} patterns. These atmospheric anomalies were characterized in a sequence of winter (January–March) anomalous surface pressure (p_a) maps for 1950–92 that had been temporally filtered to pass decadal and longer periods. These maps are presented in Fig. 1. Five high (H1 to H5) and three low (L1 to L3) pressure anomaly features dominated this long-period variability. Propagation of anomaly features was observed at times, with feature H1 propagating east-northeastward during the early and mid-1950s and features L1, H3, L2, and H4 propagating southward between 1964 and 1984 (Fig. 1). This highly nonstationary variability has been obscured in earlier atmospheric climate studies due to the reliance on statistical analysis techniques such as empirical orthogonal functions that assume stationarity and resolve only standing patterns of oscillation. Concerning the T_{sa} response (Halliwell 1997), cold (warm) anomaly features were generally observed wherever the p_a anomalies in Fig. 1 acted to produce anomalously strong (weak) winter winds. Basin-scale T_{sa} patterns qualitatively resembled anomalous surface turbulent (latent plus sensible) heat flux patterns resulting from this anomalous wind speed.

The present study is designed to provide a more ac-

Corresponding author address: Dr. George R. Halliwell, RSMAS/MPO,University of Miami, 4600 Rickenbacker Causeway, Miami, FL 33149-1098.
E-mail: ghalliwell@rsmas.miami.edu

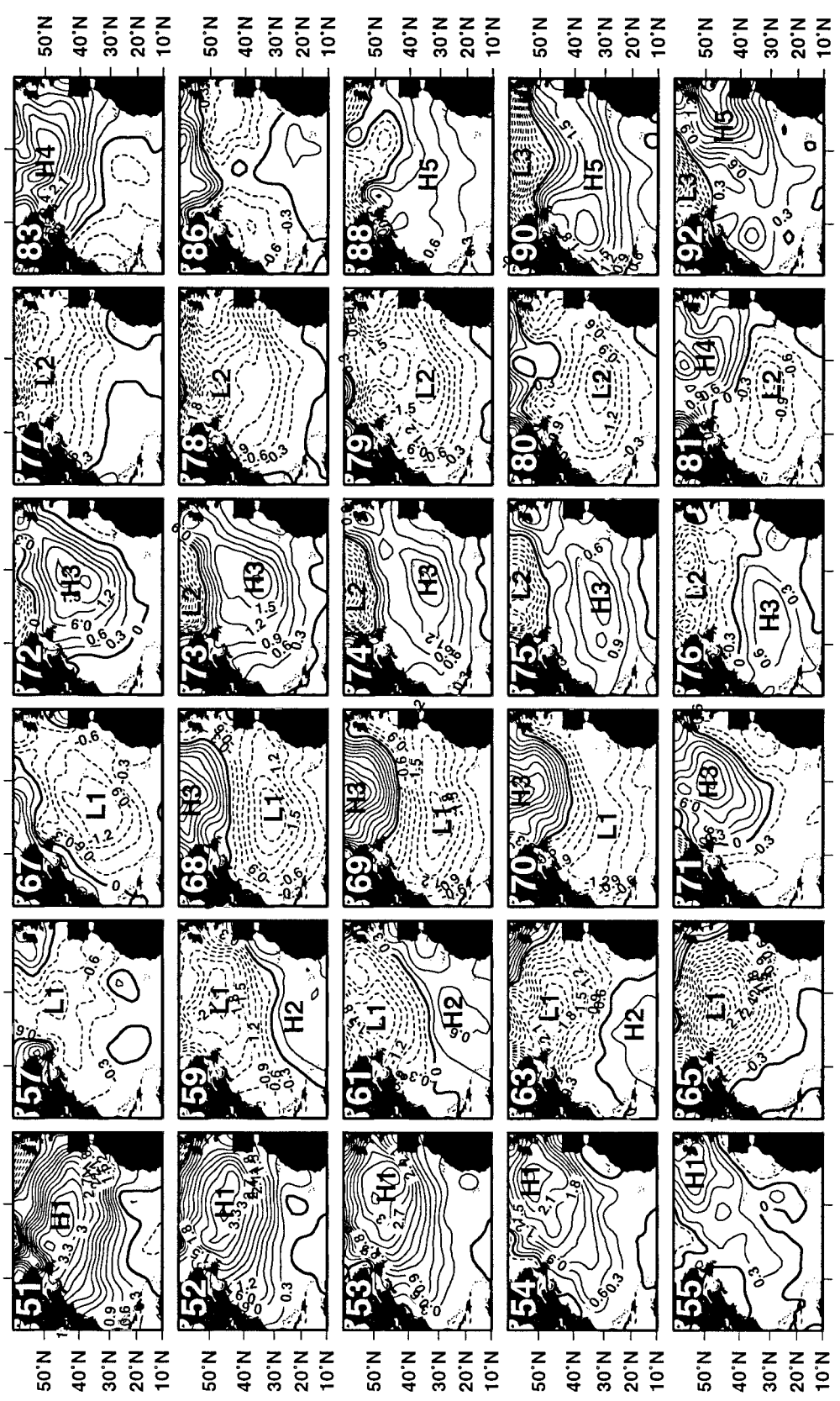

FIG. 1. Maps of observed winter (Jan–Mar) surface atmospheric pressure anomaly p_a, originally presented in Halliwell (1997). The fields were temporally filtered to remove fluctuations with periods shorter than decadal and linear trends were removed. Dashed contours indicate negative values. Thirty of the 42 years from 1951 to 1992, selected to maintain the continuity of individual anomaly features, are shown. The dominant high (H1 to H5) and low (L1 to L3) pressure anomaly features are labeled.

curate accounting of the winter T_{sa} response to the atmospheric forcing anomalies in Fig. 1, then use this information to characterize properties of T_{sa} variability not driven by the atmosphere. The T_{sa} response to atmospheric forcing was simulated using the Miami Isopycnic Coordinate Ocean Model (MICOM; Bleck et al. 1992). The simulation was performed by adding anomalous fields of wind speed and vector wind stress to the climatological annual cycle fields that drive the model. All terms of the closed model mixed layer temperature balance were archived for later diagnosis. Several other studies have employed ocean general circulation models to study T_{sa} variability, including Haney (1985) and Luksch and von Storch (1992) in the Pacific. Battisti et al. (1995) analyzed North Atlantic T_{sa} variability using a one-dimensional ocean model at each grid point (no advection). They drove T_{sa} fluctuations by adding anomalous atmospheric wind speed, temperature, and humidity to the climatological annual cycle forcing. These studies collectively demonstrate the importance of surface turbulent heat flux in driving seasonal to interannual T_{sa} variability in the open ocean, a result validated by the analysis of observations (e.g. Bjerknes 1964; Cayan 1992; Halliwell and Mayer 1996). The present model simulation differs by focusing on the response to the surface atmospheric circulation anomalies in Fig. 1. As such, it complements the study of Battisti et al. (1995).

Atmospheric forcing is analyzed within three regions where the simulation was reasonably accurate: the open-ocean westerly wind belt, the open-ocean trade wind belt, and the Gulf Stream region off the east coast of the United States. Forced T_{sa} responds primarily to local air–sea fluxes in the two open ocean regions and primarily to changes in the wind-driven subtropical gyre circulation in the Gulf Stream region. It is the structure of the atmospheric anomalies in Fig. 1 in conjunction with regional differences in dominant T_{sa} forcing mechanisms that is responsible for large-scale winter T_{sa} patterns forced by the atmosphere. After accounting for open-ocean winter T_{sa} patterns driven by the atmosphere, a single decade (1968–77) is identified where most of the North Atlantic is up to a few tenths of a degree cooler than can be accounted for by the atmospheric forcing. Both the onset and termination of this cold decade occur abruptly over an interval of about one year. This anomalously cool T_{sa} is present year-round, suggesting that the responsible forcing is relatively constant in contrast to the strong seasonal cycle of atmospheric forcing. The onset coincides with the appearance of the great salinity anomaly (Dickson et al. 1988), while the termination coincides with a sharp climate shift observed in the Pacific (e.g., Miller et al. 1994). The possibility that this cool decade occurred due to a reduction in deep-water formation, and hence in the strength of the MOC, is explored.

The presentation is organized as follows: The model simulation is described in section 2. Decadal and short-term interdecadal T_{sa} fluctuations driven by the p_a anomalies in Fig. 1 are described in section 3. A simple model relating winter T_{sa} to the integrated influence of atmospheric forcing present earlier in time is developed in section 4. The primary forcing mechanisms responsible for winter T_{sa} patterns are identified in section 5. Fluctuations in winter T_{sa} not driven by this atmospheric forcing are characterized in section 6. Notation is defined in appendix A.

2. Description of the model simulation

a. The MICOM

The thermodynamically active version of the MICOM accommodates two independent thermodynamic variables (T, S) and supports variable bottom topography and irregular coastlines; the first ocean climate study performed using this model is documented in Bleck et al. (1992). Model equations are solved on a regular (Arakawa C) grid overlying a Mercator projection, resulting in an isotropic grid resolution. The model does not use a rigid lid—it performs the barotropic and baroclinic solutions using a split-explicit scheme. The top layer is a nonisopycnic slab mixed layer with entrainment and detrainment originally governed by a Kraus–Turner (Turner and Kraus 1967) TKE balance. Model equations and solution techniques are described in Bleck et al. (1992), while the basic mixed layer model is described in Bleck et al. (1989).

The MICOM version used in the present study spans the Atlantic Ocean from about 21°S to 63°N with a horizontal grid resolution of 2° longitude and 2 $\cos\phi$° latitude and with 16 vertical layers. This version incorporates several changes to the model used by Bleck et al. (1992). It treats temperature alone as a diagnostic variable in all isopycnic layers to cut advection time in half and eliminate the need for a coordinate maintenance (''cabbeling'') algorithm. A diapycnal mixing scheme between isopycnic layers has been included that is a simplified version of the algorithm developed by Hu (1991). Model fields are relaxed to Levitus climatology within five grid points of the northern and southern boundaries. This relaxation induces a MOC of 10–15 Sv (Sv $\equiv 10^6$ m^3 s^{-1}), which is comparable to the observed magnitude. The original thermal forcing functions $\hat{T}$ and Bowen ratio have been replaced by atmospheric temperature (T_A) and humidity (q_A) fields. Concerning the mixed layer, the TKE balance of Gaspar (1988) and tested by Halliwell et al. (1994) is now employed. Mixed layer detrainment driven by surface freshwater (as opposed to heat) flux has been made easier by extending the traditional temperature redistribution method in the fossil mixed layer (Bleck et al. 1992) to a joint salinity–temperature scheme.

b. Procedure

Starting with zonally averaged Levitus (1982) climatological ocean fields as initial conditions, the model

was first run for 20 years to spin up the gyre-scale circulation. The spinup was driven by monthly climatological mean annual cycle (denoted by superscript *) fields of vector wind stress $\boldsymbol{\tau}^*$ (momentum flux), wind speed W^*, surface radiative heat flux Q_R^* (shortwave plus longwave), 10-m atmospheric temperature T_A^*, 2-m atmospheric specific humidity q_A^*, and precipitation P^*. The momentum and radiative heat fluxes are therefore directly input into the model, while the remaining air–sea fluxes are calculated by the model during run time as follows: The surface turbulent (latent plus sensible) heat flux Q_T^* is calculated using the bulk formula

$$Q_T^* = Q_L^* + Q_S^* = -\rho_A C_L L W^*(\Delta q)^* - \rho_A C_S W^*(\Delta T)^*. \quad (1)$$

The net surface mass flux ($E^* - P^*$) is determined from the input P^* field and the E^* field calculated from the latent heat flux ($E^* = Q_L^*/L$). The surface energy flux (TKE generation by the wind and surface buoyancy flux) governing mixed layer entrainment and detrainment is calculated from the momentum, heat, and mass fluxes.

Using the final model fields generated by the 20-yr spinup as initial conditions, the anomaly simulation for January 1950 through March 1992 was performed by adding the monthly anomaly (denoted by subscript a) fields of vector wind stress $\boldsymbol{\tau}_a$ and wind speed W_a to the climatological annual cycle forcing fields. As a result, an anomalous momentum flux $\boldsymbol{\tau}_a$ is directly input into the model, while the anomalous radiative heat flux Q_{Ra} is always zero. An anomalous surface turbulent heat flux ($Q_{T_a} = Q_{L_a} + Q_{S_a}$) arises from the anomalous wind speed in conjunction with model-generated T_{sa} (and hence q_{sa}), the bulk formula for which can be written as

$$Q_{T_a} = -\rho_A\{C_L L[W_a(\Delta q)^* + (W^* + W_a)q_{sa}] - C_S[W_a(\Delta T)^* + (W^* + W_a)(\Delta T)_a]. \quad (2)$$

With $P_a = 0$, anomalous mass flux results from anomalous evaporation ($E_a = Q_{L_a}/L/$). The resulting anomalous momentum, heat, and mass fluxes produce anomalous surface energy flux that affects entrainment and detrainment at the mixed layer base.

Battisti et al. (1995) drove their North Atlantic model with fields of W_a, T_{Aa}, and q_{Aa}. Fields of T_{Aa} and q_{Aa} were not used to drive the present simulation because it was run over a much larger domain containing large regions where these fields were poorly sampled (D. Mayer 1995, personal communication). Instead, it was decided to relax T_{Aa} to T_{sa} as discussed by Frankignoul (1985); that is, warm (cool) T_{sa} acts to increase (decrease) T_{Aa}. Nonzero T_{Aa} is therefore included in (2). An atmospheric model study by Kutzbach et al. (1977) suggested that $T_{Aa} \approx 0.75T_{sa}$, and this relaxation was implemented for the present simulation under the assumption that the relaxation timescale is much shorter than the seasonal resolution of the anomalous forcing. To estimate $T_{sa} = T_s - T_s^*$ during the anomaly simulation, T_s^* was obtained from the last full year of the 20-yr spinup. Since the influence of anomalous evaporation on q_{Aa} is not well known (Frankignoul 1985), no attempt was made to relax q_{Aa}, and it is not included in (2).

Data are not assimilated and simulated fields are not relaxed to climatology outside of the northern and southern boundary layers. The model mixed layer is free to develop T_s anomalies in response to the imposed anomalous wind speed and wind stress. The simulation analyzed here was compared to a simulation run without the northern and southern relaxation boundary conditions, and thus no MOC. The existence of the MOC tended to improve the simulation by causing the Gulf Stream to separate at a more realistic latitude, and by warming T^* in the northern subtropical and southern subpolar gyres. This warming increased $(\Delta T)^*$ and $(\Delta q)^*$ in these regions, allowing wind speed anomalies to drive larger T_{sa} variability. Furthermore, the existence of the MOC slightly (but not significantly) increased the correlation between simulated and observed T_{sa} over most of the North Atlantic.

The T_{Aa} relaxation also substantially increased the amplitude of the T_{sa} response to imposed wind speed anomalies, primarily in the westerly wind belt. Battisti et al. (1995) pointed out that T_{sa} oscillations driven by W_a alone are too small in the North Atlantic westerly wind belt and that forcing by T_{Aa} and q_{Aa} is necessary. The T_{Aa} fields used by Battisti et al. (1995) are influenced by both horizontal thermal advection in the atmospheric planetary boundary layer and anomalous heating/cooling by the underlying ocean surface. The latter component of T_{Aa} is largely accounted for by the relaxation imposed here, so it substantially improves the magnitude of simulated T_{sa} over the open ocean away from continents.

Although the simulation was performed over a larger domain, the present analysis focuses on the North Atlantic from 10° to 57°N, the same region analyzed by Halliwell (1997) (Fig. 1). The anomalous forcing fields were derived from monthly fields of $\boldsymbol{\tau}$ and W obtained from the Comprehensive Ocean–Atmosphere Data Set (COADS, Woodruff et al. 1987). The preliminary processing, which included the generation of seasonally averaged fields, is described in Mayer and Weisberg (1993). Anomaly fields for driving the model were generated by removing seasonal mean fields calculated over the 1950–92 time interval, then removing linear trends at each grid point to suppress artificial trends resulting from measurement system changes. Quasi-hermite time interpolation was used during the model run to interpolate the seasonal anomalous forcing fields and monthly climatological forcing fields to the model time.

c. Generation of analysis fields

During the model run, monthly averaged terms of the mixed layer temperature balance were archived along

with the midmonth values of other model fields. The mean monthly annual cycle of each simulated field was calculated and removed to generate anomaly fields. Seasonally averaged time series of each field were then generated for the 169 3-month seasons beginning winter (January through March) 1950 and ending winter 1992 since the anomalous forcing fields had only seasonal resolution. For analysis and model verification, time series of observed p_a and T_{sa} were obtained from the COADS and processed in the same manner as the anomalous forcing fields (Mayer and Weisberg 1993). The seasonal time series of all simulated and observed fields were spatially smoothed using a two-dimensional Gaussian window to suppress wavelengths smaller than several hundred kilometers.

Temporally filtered winter time series of all observed and simulated fields were generated using the same procedure employed to create the p_a maps in Fig. 1. For each field, the sequence of 43 winter fields from 1950 through 1992 was first extracted from the full seasonal time series. The winter time series for each field was temporally filtered to remove oscillations with periods shorter than decadal. Linear trends were removed to suppress climate drift from simulated fields and artificial trends due to measurement system changes from observed fields. For the purposes of the present analysis, it was considered more important to allow the model to freely develop temperature anomalies than to suppress the drift by nudging temperature toward climatology. It will be demonstrated later that model climate drift did not seriously degrade the present analysis results. Some analyses required the use of anomalous mixed layer temperature balance terms averaged over fall and winter, and also required the use of summer time series of observed and simulated T_{sa}. These additional seasonal time series were processed in the same manner as the winter time series.

3. Simulated T_{sa} variability

The temporal correlation map between observed and simulated winter T_{sa} (Fig. 2) reveals that the model simulates decadal and short-term interdecadal winter T_{sa} oscillations with reasonable skill over part, but not all, of the North Atlantic domain (Fig. 2). The correlation is generally significant north of 30°N in the central and western part of the basin, exceeding 0.8 in some regions. Significant correlation (0.7–0.9) is also observed in the trade wind belt south of 25°N. Insignificant correlation exists in the eastern part of the westerlies, in the Labrador Sea, and in the center of the subtropical gyre near 30°N. Both simulated and observed winter T_{sa} have relatively large magnitude along the northern and southern boundaries of the subtropical gyre (Fig. 2). However, the amplitude of T_{sa} is substantially underestimated by the simulation in most regions except for the trade wind belt (the southern boundary region of the subtropical gyre) and the Gulf Stream region near the U.S. coast. Importantly, correlation between observed and simulated T_{sa} was generally high in regions with large T_{sa} fluctuations. Three regions with large T_{sa} magnitude were selected for analysis: the westerly wind, trade wind, and Gulf Stream regions (Fig. 2). It is particularly important to account for atmospheric forcing within the westerly wind region because this is where model studies indicate that short-term interdecadal T_{sa} variability responds energetically to changes in oceanic circulation, in particular the MOC (e.g., Delworth et al. 1993; Cai et al. 1995).

Time series of winter T_{sa} spatially averaged over each of the three analysis regions generally reveal good agreement between observed and simulated T_{sa} (Fig. 3), emphasizing the importance of the atmospheric forcing anomalies in Fig. 1. Observed and simulated T_{sa} have similar magnitudes in both the trade wind and Gulf Stream regions (Table 1). In the westerly wind region, however, simulated T_{sa} has only 59% of the observed magnitude (Table 1). In large part due to the underestimated magnitude, simulated T_{sa} in the westerly wind region (Fig. 3a) is not as good as it is in the other two regions (Figs. 3b and 3c). All important forcing mechanisms are clearly not accounted for in the westerly wind region. This includes forcing by local processes such as anomalous atmospheric temperature and humidity fluctuations (Battisti et al. 1995); by unresolved synoptic atmospheric fluctuations (weather), which can exert a nonlinear influence on climatic T_{sa} fluctuations (e.g., Paduan and de Szoeke 1986); and by oceanic processes (section 6).

Comparing the three regions, energetic variability extends to periods of at least several decades in the Gulf Stream region, but is primarily confined to periods $\leq$20 yr in the two open ocean regions. Warm (cool) intervals in the westerly wind and trade wind regions tend to occur when the atmospheric circulation anomalies in Fig. 1 act to decrease (increase) wind speed. During 1964–84 when the p_a anomalies in Fig. 1 propagated southward, T_{sa} fluctuations are in-phase between the westerly wind and trade wind regions, and these fluctuations are out of phase with those observed in the Gulf Stream region. During the remainder of the 1950–92 time interval, variability in the three regions appears to be unrelated. The forced winter T_{sa} patterns also have nonstationary statistical properties.

The model climate drift did not significantly degrade the quality of simulated T_{sa} variability with periods of 10–40 yr. In the westerly wind region, a total simulated T_{sa} decrease of -0.71°C occurred over the 42-yr time interval (Table 2). However, the decrease in observed T_{sa} was -0.93°C, so most of the simulated temperature change was not due to an unrealistic model climate drift. The difference in the observed and simulated linear temperature changes in the trade wind region also was not large (Table 2). In contrast, a relatively large model climate drift was observed in the Gulf Stream region, where the observed linear temperature change was

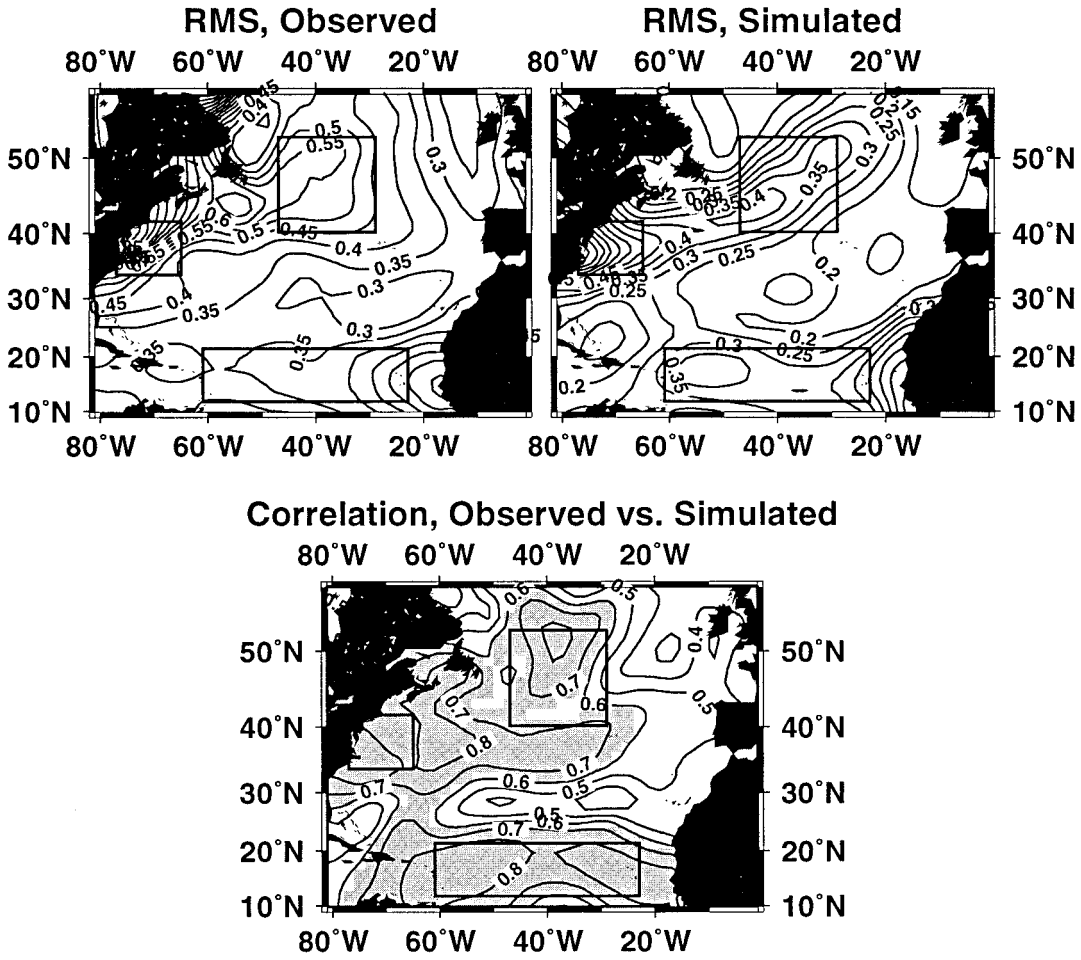

FIG. 2. Maps of the rms amplitude of observed (upper left) and simulated (upper right) winter T_{sa} along with a map of the correlation between observed and simulated T_{sa} (bottom). Shading in the bottom panel indicates statistically significant correlations to 95% confidence assuming 10 effective degrees of freedom. These correlation maps were calculated from winter time series that were temporally filtered and had linear trends removed. The three primary analysis regions are outlined by boxes and are referred to as the westerly wind region (north), trade wind region (south), and the Gulf Stream region (west).

−0.10°C and the simulated change was 0.96°C. In the model, there was a slow northward shift in the Gulf Stream path that led to the simulated T_{sa} increase. When these trends are removed, however, there is good correspondence between observed and simulated T_{sa} variability over periods of 10–40 yr (Fig. 3c). For the purposes of the present study, model climate drift did not significantly degrade the results. However, model climate drift will have to be corrected before variability with periods longer than the analysis time interval can be accurately simulated.

4. Atmospheric forcing of winter T_{sa}

a. T_{sa} balance

The model slab mixed layer anomalous temperature balance can be written as

$$\frac{\partial T_{sa}}{\partial t} = A_{Ea} + A_{Oa} + H_{ea} + H_{T_a}, \tag{3a}$$

where

$$A_{Ea} = -[(\rho f h)^{-1}\boldsymbol{\tau}\cdot\boldsymbol{\nabla}T]_a \tag{3b}$$

is the Ekman flow advection term,

$$A_{Oa} = -(\mathbf{v}_O\cdot\boldsymbol{\nabla}T)_a \tag{3c}$$

is the oceanic quasigeostrophic flow advection term,

$$H_{ea} = -(h^{-1}w_{ea}\delta_h T)_a \tag{3d}$$

is the entrainment heat flux term, and

$$H_{T_a} = -[(\rho c_p h)^{-1}Q_T]_a \tag{3e}$$

is the surface turbulent heat flux term with Q_{T_a} given by (2). Horizontal diffusion is neglected—damping of large-scale climate variability primarily results from

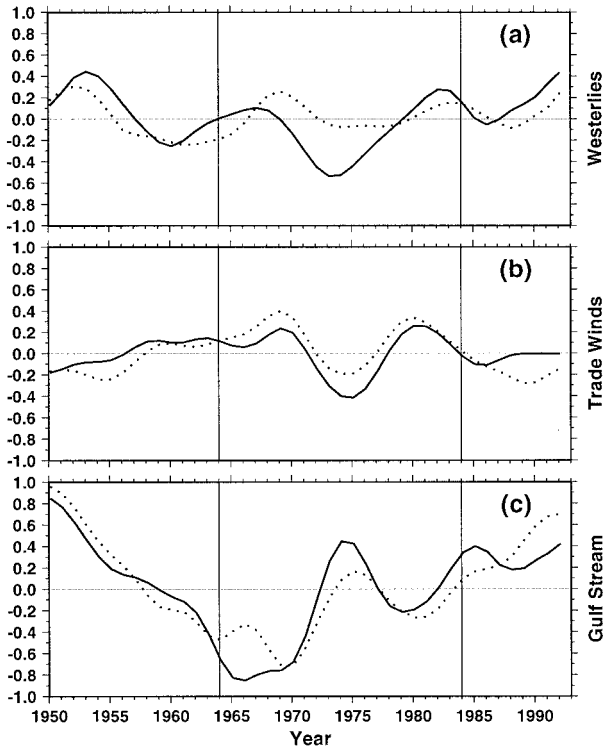

FIG. 3. Time series of observed (solid lines) and simulated (dotted lines) T_{sa} averaged over the three primary analysis regions illustrated in Fig. 2: (a) the westerly wind region (correlation $r = 0.66$), (b) the trade wind region ($r = 0.79$), and (c) the Gulf Stream region ($r = 0.89$).

negative feedback processes (Frankignoul 1985). The anomalous radiative heat flux term

$$H_{Ra} = -[(\rho c_p h)^{-1} Q_{Ra}]_a$$

is also neglected because it is small. (Although $Q_{Ra} = 0$, $H_{Ra} \neq 0$ when $h_a \neq 0$.) Anomaly terms A_{Ea}, A_{Oa}, and H_{ea} were calculated by simply subtracting the mean annual cycles from the archived monthly model terms. In contrast, H_{T_a} from (3e) was expanded into two terms. Halliwell and Mayer (1996) demonstrated that anomalous wind speed generates anomalous surface turbulent heat flux forcing primarily through the following component of H_{T_a} obtained from (2) and (3e):

$$H_{T_{a1}} = -(\rho c_p h)^{-1} \rho_A (C_L L W_a \Delta q^* + C_S W_a \Delta T^*). \quad (4)$$

Term $H_{T_{a1}}$ was calculated from (4) using monthly model fields of h, COADS fields of W_a, model fields of T_s^* (and hence q_s^*), and the climatological forcing fields of q_A^* and T_A^*. The remaining contribution $H_{Ta_2} = H_{T_a} - H_{T_{a1}}$ contributes primarily to the negative feedback damping (Halliwell and Mayer 1996). The resulting monthly fields of all terms in (3) and (4) were processed as described in section 3c.

TABLE 1. Rms amplitude of simulated winter T_{sa}, observed winter T_{sa}, and forcing terms from (7) calculated from time series averaged over the three primary analysis domains that were temporally filtered and had linear trends removed.

Parameter	Westerlies	Trade winds	Gulf Stream
Observed T_{sa} (°C)	0.22	0.14	0.38
Simulated T_{sa} (°C)	0.13	0.16	0.37
Integrated forcing (°C yr^{-1})	0.33	0.47	0.72
Ekman advection forcing (°C yr^{-1})	0.10	0.03	0.09
Oceanic advection forcing (°C yr^{-1})	0.02	0.02	0.47
Entrainment forcing (°C yr^{-1})	0.16	0.16	0.35
Turbulent heat flux forcing (°C yr^{-1})	0.27	0.34	0.13

b. Atmospheric forcing of winter T_{sa}

Relating winter T_{sa} to the atmospheric forcing is complicated by the strong seasonal cycle of atmospheric forcing. For both the atmospheric circulation anomalies in Fig. 1 and the T_{sa} patterns driven by these anomalies, conditions present during a given winter are essentially uncorrelated with conditions present during the previous summer (Fig. 4). Correlations between winter and summer T_{sa} were also calculated between several pairs of grid points spatially lagged by the cumulative flow trajectory between summer and winter (not shown). Taking mean flow advection into account did not improve the summer–winter T_{sa} correlation. Although the winter atmosphere has little memory of conditions present during the previous summer, the temporal coherence of individual p_a features in Fig. 1 demonstrates that the winter atmosphere has significant memory of conditions present during previous winters. As a result, the winter T_{sa} response to atmospheric forcing also has little memory of conditions present during the previous summer but significant memory of conditions present during previous winters. Hence, the forcing and response patterns present during a given winter both disappear by the following summer, then similar patterns re-appear by the following winter. It will be demonstrated below that the T_{sa} pattern present during a given winter represents an integrated response to the atmospheric forcing present since the beginning of the previous fall when the p_a pattern present during that winter typically begins to appear.

The pattern of T_{sa} present during a given winter does not resemble the pattern present during the previous summer for two reasons: 1) the forcing pattern present during winter usually differs substantially from the forcing pattern present during the previous summer, and 2)

TABLE 2. The T_{sa} change in the three analysis regions due to linear trends over the entire 42-yr analysis time interval.

Region	Observed T_{sa} (°C)	Simulated T_{sa} (°C)
Westerlies	−0.93	−0.71
Trade winds	−0.03	0.20
Gulf Stream	−0.10	0.96

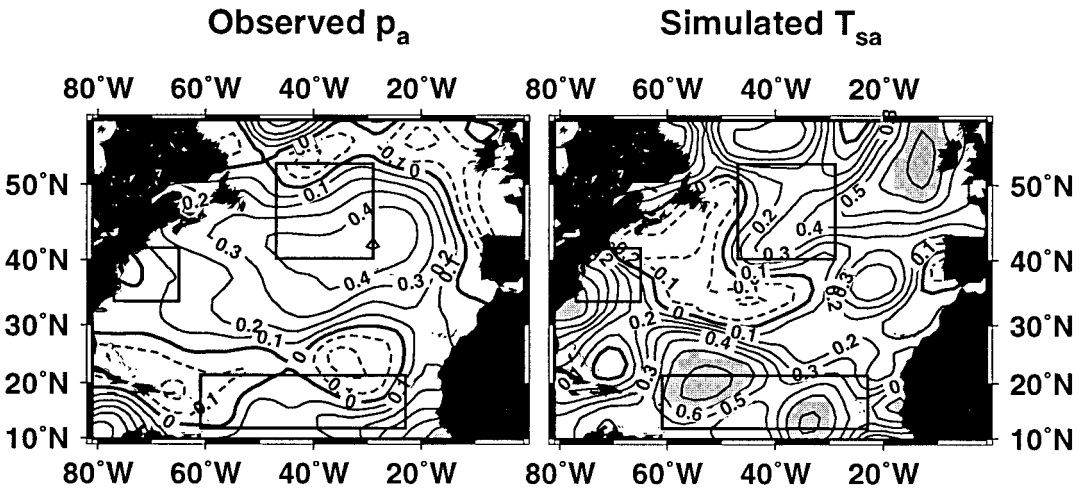

FIG. 4. Correlation between winter and summer time series of observed p_a (left) and simulated T_{sa} (right). In both cases, the winter time series begins in winter 1951 while the summer time series begins in summer 1950. Consequently, these maps represent the correlation between winter values and the values present during the previous summer, that is, a lag of -2 seasons. Shading indicates statistically significant correlations to 95% confidence assuming 10 effective degrees of freedom.

the decay timescale of forced T_{sa} fluctuations is substantially shorter than six months. The short decay timescale results primarily from negative feedback processes, primarily negative feedback with the atmosphere, that are the dominant damping mechanisms for large-scale climatic T_{sa} variability (Frankignoul 1985). The simplest model containing the influence of negative feedback damping is that of Frankignoul and Hasselmann (1977) (cf. Frankignoul 1985):

$$\frac{dT_{sa}}{dt} = +F_a - \lambda T_{sa}, \tag{5}$$

where F_a represents local forcing and $-\lambda T_{sa}$ represents negative feedback damping with decay timescale λ^{-1}. This model has been used to predict stochastic properties of the low-frequency response to synoptic atmospheric forcing (weather) (e.g., Reynolds 1979; Frankignoul and Reynolds 1983). Halliwell and Mayer (1996) demonstrated that (5) can explain observed frequency response properties of winter T_{sa} fluctuations driven by the atmosphere for periods up to at least 20 yr.

Previous studies have determined that characteristic decay timescales of SST anomalies for the midlatitude ocean are 2–3 mo (e.g., Reynolds 1979; Frankignoul and Reynolds 1983; Halliwell and Mayer 1996). Given these decay timescales, (5) predicts that T_{sa} present during a given summer will have little influence on T_{sa} present during the following winter (appendix B). The model (5) also predicts that T_{sa} present during a particular winter ($T_{sa}^{(\mathrm{win})}$) arises primarily as a cumulative response to forcing present during the previous few months. Given mixed layer anomalous temperature balance terms with seasonal resolution, the integral forcing responsible for winter T_{sa} can be estimated from (5) as described in appendix B:

$$T_{sa}^{(\mathrm{win})} \approx \frac{0.83}{\lambda}\overline{(F_a^{(\mathrm{fal})} + F_a^{(\mathrm{win})})}, \tag{6}$$

where $F_a^{(\mathrm{win})}$ is the forcing present during that winter and $F_a^{(\mathrm{fal})}$ is the forcing present during the previous fall.

To estimate the forcing in (6), it was first determined that terms A_{Ea}, A_{Oa}, H_{ea}, and $H_{T_{a1}}$ in (3) and (4) account for nearly all of the forcing since $H_{T_{a2}}$ predominantly acts as negative feedback damping (Halliwell and Mayer 1996). Since the model (5) is being analyzed as a local balance, advective forcing has been included along with the local thermodynamical forcing. Using these four terms to estimate the integrated forcing in (6),

$$T_{sa}^{(\mathrm{win})} \approx \frac{0.83}{\lambda}\Big[\overline{(A_{Ea}^{(\mathrm{fal})} + A_{Ea}^{(\mathrm{win})})} + \overline{(A_{Oa}^{(\mathrm{fal})} + A_{Oa}^{(\mathrm{win})})} + \overline{(H_{ea}^{(\mathrm{fal})} + H_{ea}^{(\mathrm{win})})} + \overline{(H_{T_{a1}}^{(\mathrm{fal})} + H_{T_{a1}}^{(\mathrm{win})})}\Big]. \tag{7}$$

If the approximation (7) is valid at a given location, then the time series of winter T_{sa} will be highly correlated and in-phase with the time series of integrated forcing. This close correspondence is observed in all three analysis regions (Figs. 5–7).

5. Forcing analysis

a. Regional analyses

In the westerly wind region, the dominant 10–20-yr oscillations present in the (temporally filtered) simulated T_{sa} time series (Fig. 5a) are largely accounted for by

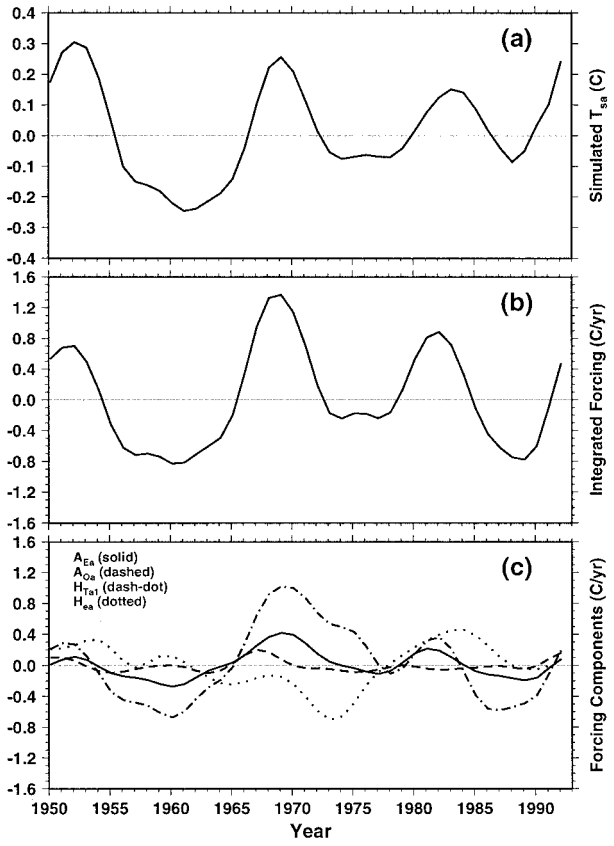

FIG. 5. Time series of (a) simulated T_a, (b) the integrated forcing from (7), and (c) the four separate terms contributing to this integrated forcing for the westerly wind analysis region.

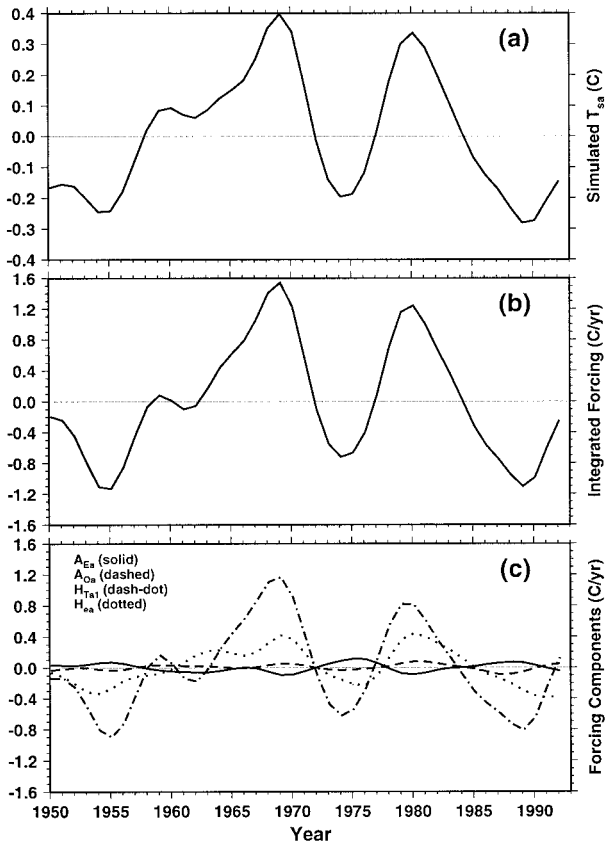

FIG. 6. As in Fig. 5 but for the trade wind analysis region.

the integrated forcing estimated from (7) (Fig. 5b). The time series of the four individual forcing terms from (7) (Fig. 5c), along with the rms amplitudes of these terms (Table 1), reveal that in decreasing order of importance, $H_{T_{a1}}$, H_{ea}, and A_{Ea} exert a significant influence on T_{sa}. The magnitudes of H_{ea} and A_{Ea} forcing equal 59% and 37% respectively of the magnitude of $H_{T_{a1}}$ forcing. Forcing by A_{Oa} has only a very small influence since it has less than 10% of the magnitude of $H_{T_{a1}}$. Terms $H_{T_{a1}}$ and A_{Ea} are highly correlated in time because anomalously strong westerlies cool the ocean both through the anomalous turbulent heat flux and through increased southward cold advection. The entrainment term H_{ea}, however, tends to be negatively correlated with both $H_{T_{a1}}$ and A_{Ea}. When T_{sa} is anomalously cool (warm), entrainment cooling tends to be anomalously weak (strong). Alexander and Deser (1995) suggested that in regions of significant annual mixed layer thickness variability, winter T_{sa} memory is provided by the fact that the previous winter temperature anomaly persists beneath the shallow summer mixed layer and reappears in the mixed layer as it deepens during the subsequent fall. The negative relationship between T_{sa} and the entrainment term observed here suggests that this mechanism is not important for decadal and longer-period variability in the westerlies. Memory of previous winters is therefore primarily provided by the atmospheric forcing.

The forcing analysis for the trade wind region again reveals a dominant 10–20-yr oscillation in simulated T_{sa} (Fig. 6a) that is largely accounted for by the integrated forcing given by (7) (Fig. 6b). The time series of the individual four forcing terms (Fig. 6c) along with the rms amplitudes of the terms (Table 1) reveal that in decreasing order of importance, H_{Ta1} and H_{ea} exert a significant influence on T_{sa}. The magnitude of H_{ea} forcing equals about 47% of the magnitude of $H_{T_{a1}}$ forcing. Both advection terms are unimportant since they have less than 10% of the magnitude of $H_{T_{a1}}$. In contrast to the westerly wind region, terms $H_{T_{a1}}$ and H_{ea} tend to be highly correlated. Anomalously strong trade winds thus act to simultaneously cool the ocean through the anomalous heat flux and to a lesser extent through anomalous entrainment. The connection between anomalous entrainment cooling and strong wind is consistent with the entrainment term depending primarily on the anomalous turbulent kinetic energy generation and anomalous surface buoyancy flux (largely resulting from anomalous evaporation) resulting from the anomalous wind speed. The mechanism of Alexander and Deser (1995) could also contribute to the positive correlation between T_{sa} and the entrainment term. This contrasts with the west-

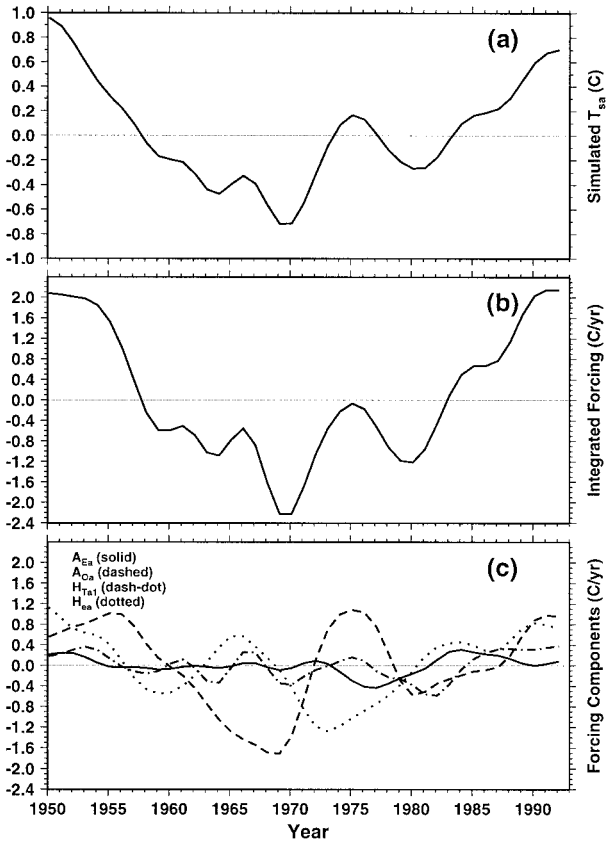

FIG. 7. As in Fig. 5 but for the Gulf Stream analysis region.

erlies where the entrainment term must depend primarily on other processes, for example, on the density and temperature jumps at the mixed layer base, on anomalous Ekman pumping, or on anomalous temperature beneath the mixed layer.

The forcing analysis for the Gulf Stream region reveals fluctuations in simulated T_{sa} dominated by periods of one to several decades (Fig. 7a) that are again largely accounted for by the integrated forcing given by (7) (Fig. 7b). The time series of the individual four forcing terms (Fig. 7c) along with the rms amplitudes of the terms (Table 1) reveal that in decreasing order of importance, A_{Oa}, H_{ea}, H_{Ta1}, and A_{Ea} all exert a significant influence on T_{sa}. The magnitudes of H_{ea}, H_{Ta1}, and A_{Ea} forcing equal about 74%, 28%, and 20%, respectively, of the magnitude of A_{Oa}. Unlike the open ocean, the dominant processes influencing T_{sa} in the Gulf Stream region are unrelated to the local anomalous wind field. The importance of A_{Oa} suggests that T_{sa} responds primarily to decadal and interdecadal changes in the strength and location of the stream associated with changes in wind-driven gyre circulation. Terms A_{Oa} and H_{ea} tend to be negatively correlated from 1957 to 1987 such that anomalous entrainment cooling is enhanced when changes in the Gulf Stream flow result in anomalous warming. As in the westerly wind region, the entrainment term apparently depends strongly on processes other than anomalous TKE generation by the wind and by surface buoyancy flux.

The fundamental difference in forcing mechanisms between the Gulf Stream region and the two open ocean regions is highlighted by correlating time series of winter T_{sa} oscillations averaged over each of these regions to time series of winter p_a maps (Fig. 8). In the westerly wind region, T_{sa} fluctuations with decadal and longer periods are significantly positively correlated with p_a oscillations centered to the north of the region. In the trade wind region, T_{sa} fluctuations with decadal and longer periods are significantly negatively correlated with p_a oscillations centered to the north of the region. These two correlation patterns can be explained by the relationship between T_{sa} and anomalous wind speed. Positive T_{sa} in the westerlies is associated with positive $\partial p_a/\partial y$ (weak westerlies), while positive T_{sa} in the trades is associated with negative $\partial p_a/\partial y$ (weak trades). Although the region of strongest wind speed fluctuations associated with the correlated p_a pattern in Fig. 8 is to the south of the westerlies analysis region, Δq^* and ΔT^* are larger in the westerlies analysis region so that from (3e) and (4), the smaller W_a there can generate relatively large T_{sa} variability.

The situation for the Gulf Stream region is entirely different with positive T_{sa} being associated with an anomalously strong subtropical high, that is, with anomalously strong Ekman downwelling over the subtropical gyre. Furthermore, the maximum correlation pattern is observed when the p_a field leads T_{sa} by 2 yr, while statistically significant correlation is observed for p_a leading by 0–5 yr, suggestive of the long baroclinic adjustment timescale of the subtropical gyre. In contrast, the largest correlations between T_{sa} in the two open ocean regions and p_a occurred for zero lag time, consistent with the 2–3 mo adjustment timescale of the mixed layer with respect to local forcing. It is remarkable that the gyre forcing can account for such a large fraction of observed T_{sa} in the Gulf Stream region considering that energetic smaller-scale, higher-frequency T_{sa} variability exists there (e.g., Kelly and Qiu 1995) that is not resolved in the present low-resolution simulation.

b. Atmospheric forcing of winter T_{sa} patterns

Simulated T_{sa} patterns were compared to the observed patterns discussed in Halliwell (1997), and reasonably good agreement was generally observed. For example, the large warm T_{sa} feature that formed to the south and southwest of p_a feature H1 where the westerlies were abnormally weak, and that propagated east-northeastward along with H1, was generated by the simulation during the early to mid-1950s (not shown). To rationalize how the atmospheric circulation anomalies in Fig. 1 drive large-scale T_{sa} patterns, the forced winter T_{sa} pattern for 1969 is analyzed in conjunction with maps

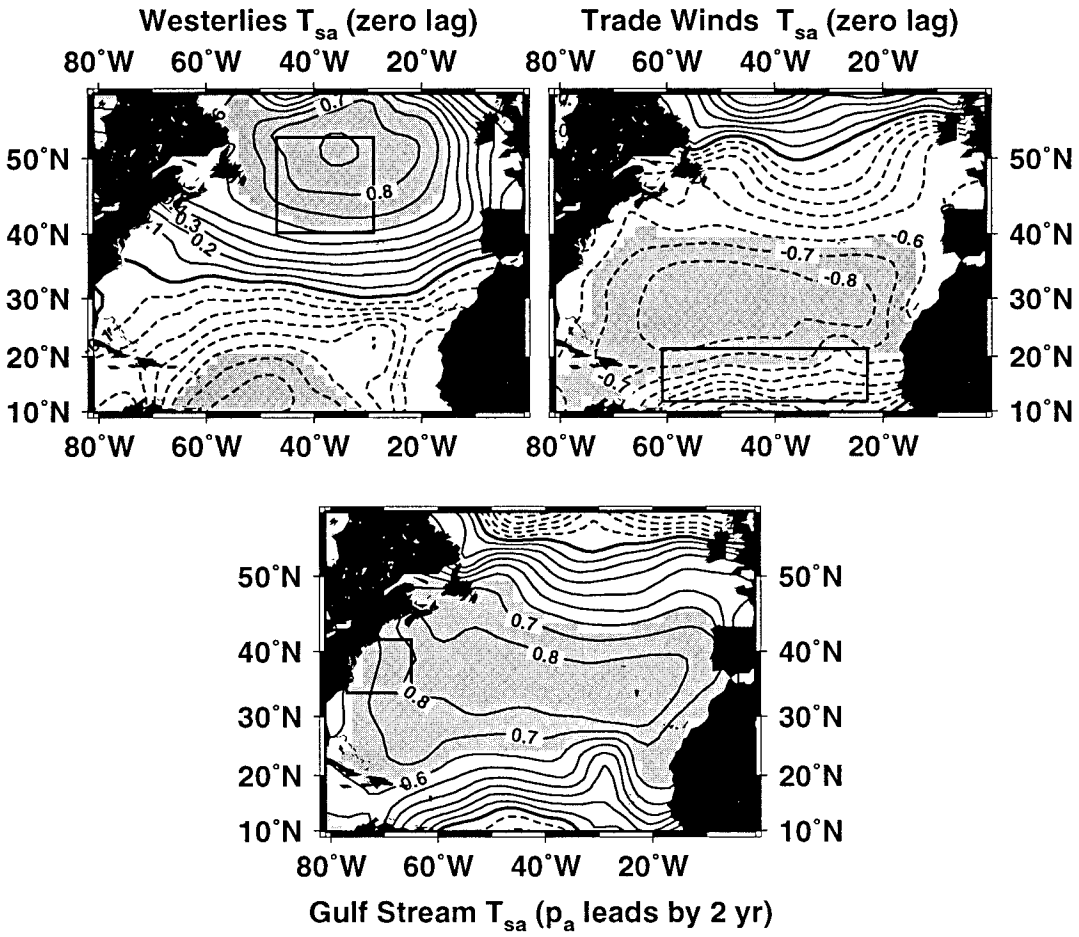

FIG. 8. Correlation between time series of winter T_{sa} averaged over the westerly wind (upper left), the trade wind (upper right), and the Gulf Stream (bottom) analysis regions and maps of p_a. The box over which T_{sa} was averaged is shown in each panel. All three correlation maps are for time lags that maximize the correlation, for zero lag in the westerly wind and trade wind regions and for p_a leading T_{sa} by 2 yr in the Gulf Stream region. Dashed contours indicate negative values. Shading indicates statistically significant correlations.

of the integrated forcing terms from (7) (Fig. 9). During 1968 and 1969, the p_a pattern in Fig. 1 is associated with an abnormally weak subtropical high and abnormally weak subpolar (Icelandic) low. Winter 1969 is considered here to allow for some of the lag of T_{sa} in the Gulf Stream region with respect to the anomalous basin-scale forcing.

The anomalously weak westerlies and trades present during 1969 were associated with positive T_{sa} over most of the open ocean North Atlantic (Fig. 9). In contrast, the anomalously weak subtropical high and the associated reduction in Ekman pumping weakened the subtropical gyre, which led to negative T_{sa} in the Gulf Stream region off the U.S. East Coast. Similar structure present in the maps of winter T_{sa} and the integrated forcing again suggests that (7) is a good approximation. The open ocean warming is largely caused by $H_{T_{a1}}$, but is supplemented by A_{Ea} in the westerlies and H_{ea} in the trades. The cooling in the model Gulf Stream is primarily due to A_{Oa}, and this region of cooling extends eastward from the U.S. coast to 50°W roughly along the model Gulf Stream axis (Fig. 9). This coincides with the region where Battisti et al. (1995) speculated that advective cooling was important since their locally forced response did not resemble observed T_{sa} variability there. Entrainment H_{ea} supplements this cooling in the Gulf Stream east of 65°W, while $H_{T_{a1}}$ acts to cool T_{sa} to the south of the model Gulf Stream west of 55°W. As a result, most of the western subtropical gyre is colder than normal.

6. T_{sa} fluctuations not driven by the atmosphere

The simulated winter T_{sa} response to atmospheric forcing can be subtracted from observed winter T_{sa} to characterize properties of decadal and short-term interdecadal winter T_{sa} fluctuations driven by other processes. Difference time series (observed minus simulated) of winter T_{sa} averaged over individual analysis regions were calculated from unfiltered time series to emphasize

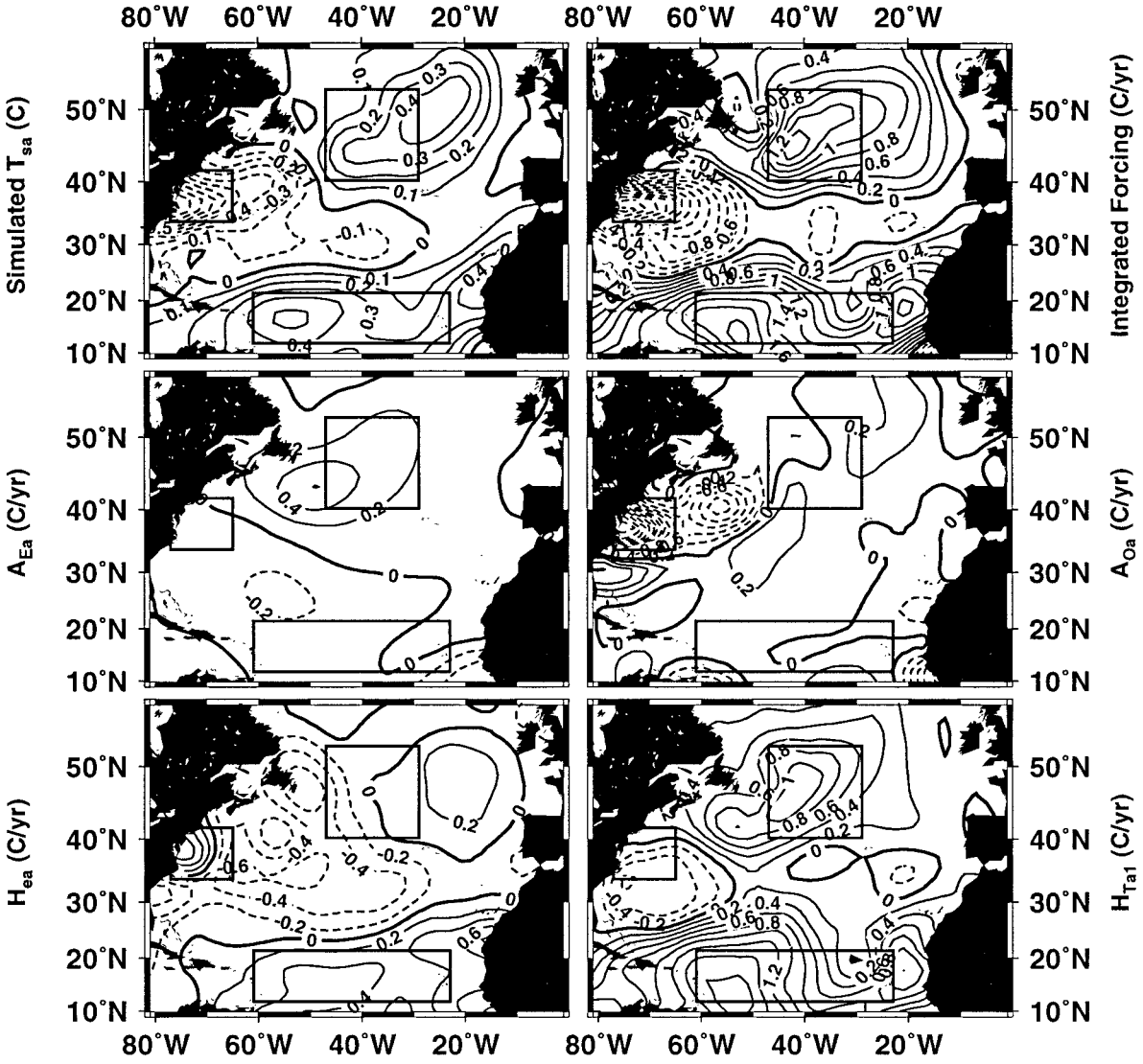

FIG. 9. Maps of simulated T_{sa} (upper left), the integrated forcing from (7) (upper right), and the four components of the integrated forcing (middle and lower panels) for winter 1969. The three analysis regions are outlined.

sharp transitions that occurred in both the late 1960s and late 1970s (Fig. 10). The winter difference time series for the westerly wind region (Fig. 10) clearly reveals a one-decade time interval from the late 1960s to the late 1970s when the ocean was anomalously cold. Both the onset and termination of this cold decade occurred abruptly within one year. A map of the average T_{sa} difference (observed minus simulated) for winter 1968 through winter 1977 presented in Fig. 11 indicates that observed T_{sa} is colder than simulated T_{sa} over nearly the entire North Atlantic. The difference is relatively large and statistically significant in a broad region to the south of the model Gulf Stream and North Atlantic Current that extends across nearly the entire basin. In addition to the westerly wind analysis domain, a difference time series was also calculated over a second region farther to the east where the mean difference is larger (Fig. 11) and atmospheric forcing is comparatively weak. The cool decade and the two abrupt transitions associated with it are more sharply defined in this eastern region than in the westerly wind region (Fig. 10).

Since simulated winter T_{sa} cannot account for the existence of this cold decade, it is tempting to conclude that ocean circulation changes, perhaps changes in the MOC, are responsible. There is nothing in COADS-derived, temporally unfiltered p_a and wind fields that hints of abrupt atmospheric changes occuring during 1968–69 or 1976–77. It is thus difficult to believe that abrupt changes could have occurred in other atmospheric fields that can influence T_{sa} such as q_{Aa}, T_{Aa}, or cloud cover. One property of this cool decade that differs from atmospherically forced T_{sa} is that cold T_{sa} is present year round (Figs. 10 and 11). The forcing that maintains the

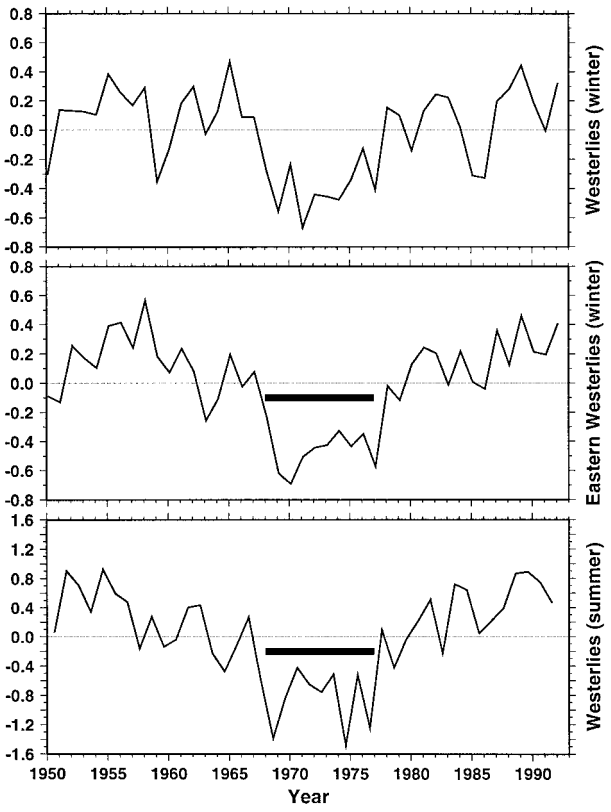

FIG. 10. Time series of observed minus simulated winter T_{sa} averaged over (a) the westerly wind analysis region and (b) a region in the eastern part of the westerly wind belt. Both of these regions are outlined in the left panel of Fig. 10. Also shown is the summer difference time series for the westerly wind analysis region (c). Horizontal bars marks the cold decade that cannot be explained by atmospheric forcing. These time series were not temporally filtered.

cool water during this decade must therefore remain relatively constant throughout the year in contrast to the strong seasonal cycle present in the atmospheric forcing. The summer difference time series in the westerly wind region (Fig. 10) also displays the same rapid onset and termination evident during winter.

The onset of the cooling during 1968 roughly coincided with the appearance of the great salinity anomaly (Dickson et al. 1988) and a probable decrease in the North Atlantic deep-water formation rate. Although the assumption that a reduction in the MOC forced this cooling cannot be proven here, it is supported by studies of interpentadal changes of the baroclinic structure and circulation of the North Atlantic that occurred from 1955–59 to 1970–74, with the latter pentad contained within the cold decade. Significant changes in the thermohaline structure of the North Atlantic occurred between these pentads (e.g., Levitus 1989). Although substantial uncertainties exist, diagnostic studies of these interpentadal changes (e.g., Greatbatch et al. 1991; Greatbatch and Xu 1993; Ezer et al. 1995) reveal that Gulf Stream transport was about 30 Sv weaker during the 1970–74 pentad, and also suggest that changes in thermohaline ocean circulation were largely responsible for these interpentadal changes.

A rough picture of the temporal evolution of T_{sa} associated with the cool decade is obtained by comparing winter T_{sa} difference maps (observed minus simulated) for the first and last halves of that decade (Fig. 12). From 1968 to 1972, the cooling was primarily confined to the northern part of the subtropical gyre south of the Gulf Stream and North Atlantic Current system. A cold tongue appears to extend northeastward off the west coast of Europe. From 1973 to 1977, the cooling appeared to spread over much of the southern subpolar

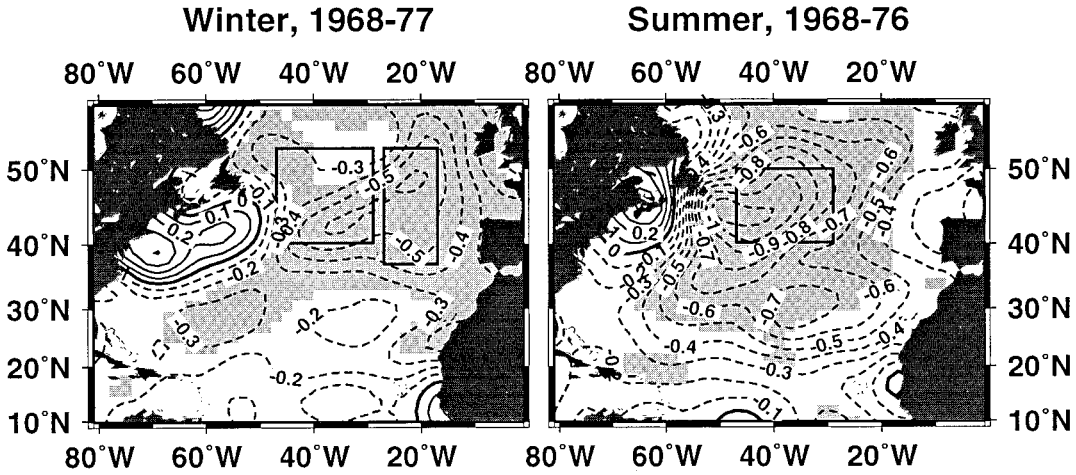

FIG. 11. Difference between observed and simulated T_{sa} averaged over all winters from 1968 through 1977 (left) and averaged over all summers from 1969 through 1976 (right). Dashed contours indicate negative values. The two boxes in the left panel are the two averaging regions for the winter T_{sa} difference time series in Fig. 9. The box in the right panel is the averaging region for the summer T_{sa} difference time series in Fig. 11. Regions where observed and simulated mean T_{sa} are significantly different to 90% confidence based on a Student's t-test are shaded.

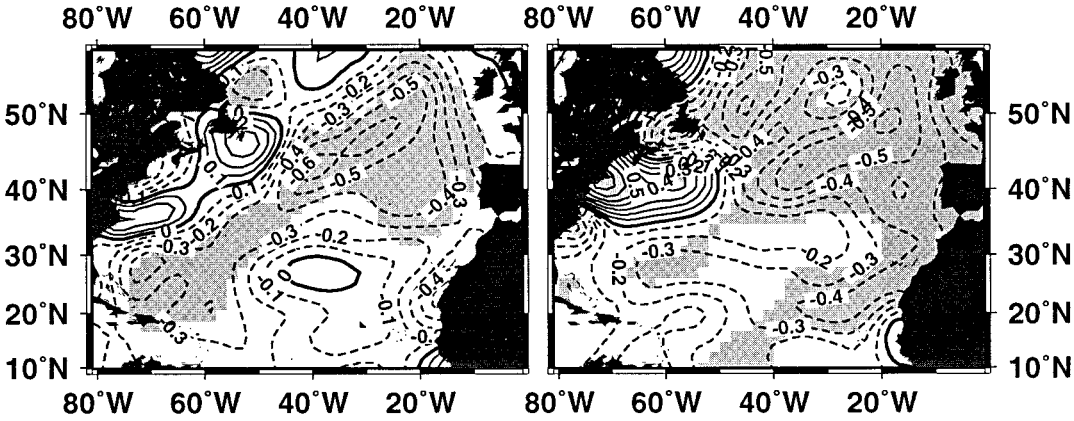

FIG. 12. Difference between observed and simulated winter T_{sa} averaged over all winters from 1968 through 1972 (left) and averaged over all winters from 1973 through 1977 (right). Dashed contours indicate negative values. Regions where observed and simulated mean T_{sa} are significantly different to 90% confidence are shaded.

gyre and around the eastern and southern limb of the subtropical gyre. Although the statistical significance of the cooling along the southern boundary of the subtropical gyre (within the trade wind belt) is questionable, the overall change in the cool water pattern is consistent with less heat being advected around the eastern limbs of both the subtropical and subpolar gyres. Furthermore, similar propagation of this cool anomaly was observed in the analysis of Hansen and Bezdek (1996). This change is consistent with reduced flow leaving the subtropical gyre to enter the eastern limb of the subpolar gyre and with enhanced flow occurring around the eastern and southern limb of the subtropical gyre, both consistent with a reduced MOC.

Whatever was responsible for the cool decade, the abrupt appearance and disappearance of this anomaly suggests that the North Atlantic jumped rather abruptly between two distinct climatic states. The abrupt warming that terminated the cool decade occurred between winter 1977 and summer 1977 (Fig. 10). It roughly coincided with a sharp climate change that occurred in the Pacific (e.g., Miller et al. 1994) and with a very cold winter in eastern North America. The extent to which the Atlantic climate shift may have been connected to the global climate shift cannot be determined here.

7. Discussion

Decadal and short-term interdecadal winter T_{sa} variability driven by the atmospheric circulation anomalies in Fig. 1 was simulated with reasonable success using an ocean general circulation model. By adding anomalous wind speed and vector wind stress to the climatological annual cycle forcing, a substantial fraction of the observed variability could be accounted for in three regions: the open-ocean westerly wind belt, the open-ocean trade wind belt, and the Gulf Stream region off the east coast of the United States. A partial relaxation of the anomalous surface atmospheric temperature to the anomalous ocean surface temperature was necessary to allow ocean temperature anomalies of reasonable magnitude to develop, in particular in the westerlies. The simulation was least successful in the westerlies analysis region, due in part to the neglect of atmospheric temperature and humidity forcing and also to the use of forcing fields that did not resolve energetic synoptic atmospheric forcing. The existence of substantial T_{sa} variability that was apparently not locally driven by the atmosphere also limited the quality of simulated T_{sa} in the westerlies. Because of these limitations, simulated T_{sa} in the westerlies has only 59% of the magnitude of observed T_{sa}. Overall, the degree of success was encouraging considering the COADS anomalous wind speed and vector wind stress fields used to force the model are noisy (e.g., Michaud and Lin 1992) and also considering that a low-resolution ocean model was used. It was possible to demonstrate how wind speed and vector wind stress anomalies alone can act to generate a substantial fraction of observed T_{sa} variability in all three regions.

The year-to-year persistence of the individual winter atmospheric circulation anomaly features in Fig. 1 along with the T_{sa} patterns driven by these anomalies (not shown) demonstrates that both the atmosphere and the T_{sa} response have significant memory of conditions present during earlier winters. In contrast, both the atmospheric anomalies and the T_{sa} response present during a given winter have little memory of conditions present during the previous summer. Consequently, the atmospheric anomalies and associated T_{sa} patterns present during a given winter tend to disappear by the following summer, then similar patterns reappear during the subsequent fall and winter. Since the winter atmospheric anomalies in Fig. 1 typically become established during the previous fall, the T_{sa} anomaly pattern present during a given winter essentially arises as an integrated response to the anomalous atmospheric forcing pattern present during that winter and the previous fall. By using

a simple model to estimate the integrated forcing responsible for T_{sa} during each winter, it was possible to quantify the relative influence of advection by the ageostrophic Ekman flow, advection by the oceanic quasigeostrophic flow, entrainment, and the anomalous surface turbulent heat flux arising from anomalous wind speed on T_{sa} in each region.

Decadal and short-term interdecadal variability in winter T_{sa} patterns driven by the atmosphere arise due to the anomalous air–sea flux patterns associated with the p_a anomalies in Fig. 1 in conjunction with regional differences in the dominant mixed layer processes that drive T_{sa}. In the two open ocean regions (the westerly wind and trade wind regions), T_{sa} is driven primarily by anomalous local air–sea flux forcing. The anomalous surface turbulent heat flux arising from the anomalous wind speed is the most important forcing mechanism in both of these regions. Smaller but significant forcing is provided by entrainment in both regions and Ekman flow in the westerlies. In the Gulf Stream region, however, T_{sa} was associated with changes in the wind-driven subtropical gyre circulation forced by basin-scale atmospheric circulation anomalies. Changes in horizontal heat advection by the oceanic flow along with anomalous entrainment heat flux associated with adjustments in the vertical density and temperature structure at and beneath the base of the mixed layer were primarily responsible for driving T_{sa} in this region. As a result, whenever the p_a features in Fig. 1 were aligned such that the subtropical high and subpolar low were both anomalously weak (e.g., 1968–69), the open ocean regions were anomalously warm due to reduced wind speeds in the westerlies and trades, while the Gulf Stream region was anomalously cool in response to adjustments in the structure and circulation of the subtropical gyre associated with anomalously weak Ekman pumping over the gyre. Opposite phases of this pattern were observed about every six years between 1964 and 1984 as the p_a anomalies in Fig. 1 propagated southward. During these two decades, T_{sa} in the Gulf Stream region was out of phase with T_{sa} in the other two regions. During the remainder of the 1950–92 time interval, a clear relationship did not exist between T_{sa} in the Gulf Stream and T_{sa} in the other two regions. Fluctuations in T_{sa} driven by the atmospheric anomalies in Fig. 1 were dominated by periods of 10–20 yr in the two open ocean regions, but were dominated by longer periods up to several decades in the Gulf Stream region.

Although simulated T_{sa} variability was not perfect, especially in the westerlies, it was sufficiently accurate to take a first look at decadal and short-term interdecadal T_{sa} variability not driven by the atmospheric anomalies in Fig. 1. When simulated winter T_{sa} was subtracted from observed T_{sa}, a decade-long cold event occurred that was characterized by a comparatively rapid onset and termination. Anomalously cold water not driven by the atmosphere was evident year-round in contrast to the strong annual cycle of atmospheric forcing and the associated T_{sa} response. The cool anomaly onset coincided with the appearance of the great salinity anomaly, so the possibility exists that this cool decade was a response to a reduction in North Atlantic deep-water formation and thus a reduction in the upper-ocean northward heat transport by the MOC. If further study proves this to be the case, then T_{sa} in the westerly wind belt can, after removing the direct response to local anomalous air–sea fluxes, be used as an indicator of the strength of the MOC. This contrasts with the Gulf Stream region off the U.S. East Coast, which can serve as an indicator of interdecadal variability in wind-driven gyre circulation.

To accurately monitor the short-term interdecadal T_{sa} variability associated with oceanic thermohaline circulation changes, we must improve our capability of simulating the oceanic response to the atmosphere through model improvements and by driving the models with improved forcing fields. However, coupled ocean–atmosphere models will ultimately be required to fully understand the phenomena described in the present analysis. The ocean clearly responds to the the atmospheric circulation anomalies in Fig. 1. The unanswered question is what provides the atmospheric memory from winter to winter that is evident in Fig. 1? Presumably, land–ocean–atmosphere–ice interactions are ultimately responsible since the internal dynamics of the atmosphere alone cannot account for this winter memory. Only one component of this interaction, the ocean response to the atmosphere, was documented here. It is not clear to what extent Atlantic T_{sa} patterns drive the atmospheric variability. For example, the mechanism of Alexander and Deser that would provide a long memory to winter T_{sa} patterns was clearly not important in the North Atlantic westerly wind belt. Instead, North Atlantic T_{sa} generally appears to respond passively to the atmospheric forcing, which is primarily responsible for the winter-to-winter memory of T_{sa}. One exception is the warm T_{sa} feature described by Halliwell (1997) that propagated east-northeastward in tandem with the p_a feature H1 in Fig. 1, suggesting that this may be a coupled phenomenon. Also, zonally symmetric, southward propagating atmospheric pressure modes were observed over a broad range of frequencies in a simulation of the ocean–atmosphere system (Mehta 1992). Although this linearized model analysis did not capture the detailed structure and amplitude of the southward propagating p_a features in Fig. 1 from 1964 to 1984, the existence of a quasi-decadal southward propagating mode in this simulation suggests that ocean–atmosphere interactions could be responsible for the observed propagation. Analysis of coupled climate models, or of fields generated from ongoing atmospheric reanalysis projects, will be required to understand the origin of the atmospheric circulation anomalies in Fig. 1.

Acknowledgments. The support of the NOAA Atlantic Climate Change Program under Grant NA90RAH00075

and NASA under Grant NAGW-4329. The author thanks C. Rooth and D. Mayer for helpful discussions.

APPENDIX A

Notation

A_{Ea}	Ekman flow advection term of the T_{sa} balance
A_{Oa}	Oceanic quasigeostrophic flow advection term of the T_{sa} balance
C_L	Bulk latent heat exchange coefficient
C_S	Bulk sensible heat exchange coefficient
c_p	Specific heat of seawater at constant pressure
E	Evaporation rate
F_a	Net local anomalous forcing
f	Coriolis parameter
H_{ea}	Entrainment heat flux term of the T_{sa} balance
H_{Ra}	Surface radiative heat flux term of the T_{sa} balance
H_{T_a}	Surface turbulent heat flux term of the T_{sa} balance
$H_{T_{a1}}$	Forcing component of H_{Ta}
$H_{T_{a2}}$	Negative feedback damping component of H_{Ta}
h	Mixed layer thickness
L	Latent heat of evaporation
λ	Inverse decay timescale for T_s anomalies
P	Precipitation rate
p	Surface atmospheric pressure
ϕ	Latitude
Q_L	Surface latent heat flux
Q_R	Surface radiative heat flux
Q_S	Surface sensible heat flux
Q_T	Surface turbulent (latent plus sensible) heat flux
q_A	10-m atmospheric specific humidity
q_s	Surface saturation specific humidity (a function of T_s)
Δq	$(=q_s - q_A)$
ρ	Bulk mixed layer density
ρ_A	Surface atmospheric density
T_A	10-m atmospheric temperature
T_{h+}	Temperature just beneath the mixed layer
T_s	Sea surface temperature, assumed to equal bulk mixed layer temperature
ΔT	$(=T_s - T_A)$
$\delta_h T$	$(=T_s - T_{h+})$
$\boldsymbol{\tau}$	Vector wind stress (momentum flux)
$\mathbf{v}_E$	Mixed layer Ekman flow velocity
$\mathbf{v}_O$	Mixed layer oceanic quasigeostrophic flow velocity
$\mathbf{v}$	$(=\mathbf{v}_E + \mathbf{v}_O)$
W	Wind speed
w_e	Entrainment velocity at the mixed layer base.

APPENDIX B

Relating Winter T_{sa} to the Forcing

The simple model (5) is used to explain the observation than winter T_{sa} is not related to T_{sa} present during the previous summer, and also to estimate the integrated forcing responsible for winter T_{sa}. The decay timescale λ^{-1} will be assumed constant since good results have been obtained with this assumption in earlier studies (e.g., Frankignoul and Reynolds 1983; Halliwell and Mayer 1996). The solution to (5) can then be written as

$$T_{sa}(t) = e^{-\lambda t}T_{sa}(0) + e^{-\lambda t}\int F_a e^{\lambda t}\, dt. \qquad \text{(B1)}$$

It is assumed that the onset of winter conditions starts at the beginning of fall, and also that temperature T_{sa} present at the beginning of fall equals the summer temperature $T_{sa}^{(\text{sum})}$. Given forcing time series of seasonal resolution and defining $t = 0$ to be the beginning of fall, the temperature present at the end of fall is estimated from (B1) to be

$$T_{sa}(3) = e^{-3\lambda}T_{sa}^{(\text{sum})} + (1 - e^{-3\lambda})\frac{F_a^{(\text{fal})}}{\lambda}, \qquad \text{(B2)}$$

where t is given in units of months and $F_a^{(\text{fal})}$ is the fall anomalous forcing. For $3 \le t \le 6$ mo, $T_{sa}(t)$ is given by

$$T_{sa}(t) = e^{-\lambda t}T_{sa}^{(\text{sum})} + (e^{3\lambda} - 1)e^{-\lambda t}\frac{F_a^{(\text{fal})}}{\lambda} + (1 - e^{-\lambda(t-3)})\frac{F_a^{(\text{win})}}{\lambda}. \qquad \text{(B3)}$$

Averaging (B3) over $3 \le t \le 6$ and assuming that $\lambda^{-1} = 2.5$ mo, $T_{sa}^{(\text{win})}$ can be estimated as

$$T^{(\text{win})} = 0.17T^{(\text{sum})} + \frac{1}{\lambda}(0.41F_a^{(\text{fal})} + 0.42F_a^{(\text{win})}). \qquad \text{(B4)}$$

The T_{sa} present during the previous summer has little effect on T_{sa} during the following winter and will be neglected. Furthermore, T_{sa} present during a given winter results primarily from integrated forcing roughly equal to $0.83/\lambda$ times the average forcing present during that winter and the previous fall, which is the justification for the approximation (6).

REFERENCES

Alexander, M. A., and C. Deser, 1995: A mechanism for the recurrence of wintertime midlatitude SST anomalies. *J. Phys. Oceanogr.*, **25,** 122–137.

Battisti, D. S., U. S. Bhatt, and M. A. Alexander, 1995: A modeling study of the interannual variability in the wintertime North Atlantic Ocean. *J. Climate*, **8,** 3067–3083.

Bjerknes, J., 1964: Atlantic air–sea interaction. *Advances in Geophysics*, Vol. 10, Academic Press, 1–82.

Bleck, R., H. P. Hanson, D. Hu, and E. P. Kraus, 1989: Mixed layer–thermocline interaction in a three-dimensional isopycnic-coordinate model. *J. Phys. Oceanogr.*, **19,** 1417–1439.

——, C. Rooth, D. Hu, and L. T. Smith, 1992: Salinity-driven thermocline transients in a wind- and thermohaline-forced isopycnic coordinate model of the North Atlantic. *J. Phys. Oceanogr.*, **22,** 1486–1505.

Cai, W., R. J. Greatbatch, and S. Zhang, 1995: Interdecadal variability in an ocean model driven by a small, zonal redistribution of the surface buoyancy flux. *J. Phys. Oceanogr.*, **25,** 1998–2010.

Cayan, D. A., 1992: Latent and sensible heat flux anomalies over the

northern oceans: Driving the sea surface temperature. *J. Phys. Oceanogr.,* **22,** 859–881.

Delworth, T., S. Manabe, and R. J. Stouffer, 1993: Interdecadal variations of the thermohaline circulation in a coupled ocean–atmosphere model. *J. Climate,* **6,** 141–157.

Deser, C., and M. L. Blackmon, 1993. Surface climate variations over the North Atlantic Ocean during winter, 1900–1989. *J. Climate,* **6,** 1743–1753.

Dickson, R. R., J. Meincke, S.-A. Malmberg, and A. J. Lee, 1988: The ''Great Salinity Anomaly'' in the northern North Atlantic, 1968–82. *Progress in Oceanography,* Vol. 20, Pergamon, 103–151.

Ezer, T., G. L. Mellor, and R. J. Greatbatch, 1995: On the interpentadal variability of the North Atlantic Ocean: Model-simulated changes in transport, meridional heat flux, and coastal sea level between 1955–59 and 1970–74. *J. Geophys Res.,* **100,** 10 559–10 566.

Frankignoul, C., 1985: Sea surface temperature anomalies, planetary waves, and air–sea feedback in the middle latitudes. *Rev. Geophys.,* **23,** 357–390.

——, and K. Hasselmann, 1977: Stochastic climate models II, application to sea surface temperature variability and thermocline variability. *Tellus,* **29,** 284–305.

——, and R. W. Reynolds, 1983: Testing a dynamical model for midlatitude sea-surface temperature anomalies. *J. Phys. Oceanogr.,* **13,** 1131–1145.

Gaspar, Ph., 1988: Modeling the seasonal cycle of the upper ocean. *J. Phys. Oceanogr.,* **18,** 161–180.

Greatbatch, R. J., and J. Xu, 1993: On the transport of volume and heat through sections across the North Atlantic: Climatology and the pentads 1955–59, 1970–74. *J. Geophys Res.,* **98,** 10 125–10 143.

——, A. F. Fanning, A. D. Goulding, and S. Levitus, 1991: A diagnosis of interpentadal circulation changes in the North Atlantic. *J. Geophys Res.,* **96,** 22 009–22 023.

Halliwell, G. R., Jr., 1997: Decadal and multidecadal North Atlantic SST anomalies driven by standing and propagating basin-scale atmospheric anomalies. *J. Climate,* **10,** 2405–2411.

——, and D. A. Mayer, 1996: Frequency response properties of forced climatic SST anomaly variability in the North Atlantic. *J. Climate,* **9,** 3575–3587.

——, F. Horsfall, R. Bleck, and H. P. Hanson, 1994: Sensitivity of an isopycnic-coordinate OGCM to parameterizations of upper-ocean mixing. *Eos, Trans. Amer. Geophys. Union,* **75**(3), 189.

Haney, R. L., 1985: Midlatitude sea surface temperature anomalies: A numerical hindcast. *J. Phys. Oceanogr.,* **15,** 787–799.

Hansen, D. V., and H. Bezdek, 1996: On the nature of decadal anomalies in North Atlantic sea surface temperature. *J. Geophys. Res.,* **101,** 8749–8758.

Hu, D.-M., 1991: Diapycnal mixing in a joint mixed-layer / isopycnic coordinate numerical model of the wind- and thermohaline-driven ocean general circulation. Ph.D. dissertation, Rosenstiel School of Marine and Atmospheric Science, University of Miami, 202 pp. [Available from University of Miami, 4600 Rickenbacker Cswy., Miami, FL, 33149-1098.]

Kelly, K. A., and B. Qiu, 1995: Heat flux estimates for the western North Atlantic. Part II: The upper-ocean heat balance. *J. Phys. Oceanogr.,* **25,** 2361–2373.

Kushnir, Y., 1994: Interdecadal variations in North Atlantic sea surface temperature and associated atmospheric conditions. *J. Climate,* **7,** 141–157.

Kutzbach, J. E., R. M. Chervin, and D. D. Houghton, 1977: Response of the NCAR general circulation model to prescribed changes in ocean surface temperature. *J. Atmos. Sci.,* **34,** 1200–1213.

Levitus, S., 1982: *Climatological Atlas of the World Ocean.* NOAA Prof. Paper No. 13, National Oceanic and Atmospheric Administration, 173 pp.

——, 1989: Interpentadal variability of temperature and salinity at intermediate depths in the North Atlantic Ocean, 1970–74 versus 1955–59. *J. Geophys. Res.,* **94,** 6091–6132.

Luksch, U., and H. von Storch, 1992: Modeling the low frequency sea surface temperature in the North Pacific. *J. Climate,* **5,** 893–906.

Mayer, D. A., and R. H. Weisberg, 1993: A description of COADS surface meteorological fields and the implied Sverdrup transports for the Atlantic Ocean from 30°S to 60°N. *J. Phys. Oceanogr.,* **23,** 2201–2221.

Mehta, V. M., 1992: Meridionally propagating interannual-to-interdecadal variability in a linear ocean–atmosphere model. *J. Climate,* **5,** 330–342.

Michaud, R., and C. A. Lin, 1992: Monthly summaries of merchant ship surface marine observations and implications for climate variability studies. *Climate Dyn.,* **7,** 45–55.

Miller, A. J., D. R. Cayan, T. P. Barnett, N. E. Graham, and J. M. Oberhuber, 1994: Interdecadal variability of the Pacific Ocean: Model response to observed heat flux and wind stress anomalies. *Climate Dyn.,* **9,** 287–302.

Paduan, J. D., and R. A. de Szoeke, 1986: Heat and energy balances in the upper ocean at 50°N, 140°W during November 1980 (STREX). *J. Phys. Oceanogr.,* **16,** 25–38.

Reynolds, R. W., 1979: A stochastic forcing model of sea surface temperature anomalies in the North Pacific and North Atlantic. Rep. 8, Climate Research Institute, Oregon State University, Corvallis, OR, 23 pp.

Turner, J. S., and E. B. Kraus, 1967: A one-dimensional model of the seasonal thermocline II: The general theory and its consequences. *Tellus,* **19,** 98–105.

Woodruff, S. D., R. J. Slutz, R. L. Jenne, and P. M. Steurer, 1987: A comprehensive ocean-atmosphere data set. *Bull. Amer. Meteor. Soc.,* **68,** 1239–1250.

Zorita, E., V. Kharin, and H. von Storch, 1992: The atmospheric circulation and sea surface temperature in the North Atlantic area in winter: Their interaction and relevance for Iberian precipitation. *J. Climate,* **5,** 1097–1108.